

# Light-Actuated AC Electroosmosis for Nanoparticle Manipulation

Pei-Yu Chiou, *Member, IEEE*, Aaron T. Ohta, *Student Member, IEEE*, Arash Jamshidi, Hsin-Yi Hsu, and Ming C. Wu, *Fellow, IEEE*

**Abstract**—We present a novel light-actuated ac electroosmosis (LACE) mechanism that allows the concentration and transportation of micro- and nanoscopic particles using light-patterned dynamically reconfigured microfluidic vortices on a photoconductive surface. LACE is realized by sandwiching an aqueous liquid medium between a featureless photoconductive surface and a transparent indium tin oxide electrode. By applying an ac electrical bias with a frequency that is close to the electric double-layer relaxation frequency, a light-patterned virtual electrode can induce ac electroosmotic flow to concentrate and transport nanoscopic particles on the photoconductive surface. By integrating with a spatial light modulator such as a digital micromirror device microdisplay, we can create 31 000 microfluidic vortices on a  $1.3 \times 1\text{-mm}^2$  area for massively parallel trapping of 2- and  $1\text{-}\mu\text{m}$  polystyrene beads. We have also demonstrated LACE concentration and transportation of nanoscopic particles including 200- and 50-nm polystyrene beads,  $\lambda$ -phage DNA molecules, and quantum dots. [2007-0197]

**Index Terms**—Dielectrophoresis (DEP), electroosmosis, electrophoresis, lab-on-a-chip, optoelectronic tweezers.

## I. INTRODUCTION

**T**OOLS FOR manipulating cells, microparticles, and nanoparticles are important in the fields of biological and colloid science. Functions such as trapping, concentrating, sorting, and transporting are highly sought after. To effectively manipulate nanoscale particles, strong field strength is necessary to form stable traps to overcome the strong Brownian motions of nanoparticles, particularly for the cases of optical tweezers [1], [2], dielectrophoresis (DEP) [3], [4], optoelectronic tweezers [5], and magnetic tweezers [6], [7] that give trap forces that are proportional to the volume of the trapped particles. When particle size scales down to the nanometer scale, strong fields are needed, and this often imposes limitations on manipulations. For example, a strong optical field could damage a spatial light modulator used for shaping a light beam; a strong electric field used in DEP traps could induce electrolysis that changes the

Manuscript received August 6, 2007; revised November 14, 2007. This work was supported in part by the Institute for Cell Mimetic Space Exploration (CMISE), a NASA University Research, Engineering, and Technology Institute (URETI), and in part by the Graduate Research and Education in Adaptive Bio-Technology (GREAT) Training Program. Subject Editor C. Ahn.

P.-Y. Chiou is with the Mechanical and Aerospace Engineering Department, University of California, Los Angeles, CA 90095 USA (e-mail: pychiou@seas.ucla.edu).

A. T. Ohta, A. Jamshidi, H.-Y. Hsu, and M. C. Wu are with the University of California, Berkeley, CA 94720 USA.

Color versions of one or more of the figures in this paper are available online at <http://ieeexplore.ieee.org>.

Digital Object Identifier 10.1109/JMEMS.2008.916342

local chemical composition or could create Joule heating that raises the local temperature.

On the other hand, ac electroosmosis has recently been demonstrated to be capable of manipulating nanoscale particles with low electric-field strength. Wong *et al.* [8] have utilized ac electroosmosis to concentrate a variety of nanoscale particles and biomolecules including *E. coli* bacteria,  $\lambda$ -phage DNA, and 20-base single-strand DNA fragments with electric-field strength on the order of  $10^4$  V/m.

In this paper, we present a light-actuated ac electroosmosis (LACE) mechanism that allows optically patterned microfluidic vortices and self-aligned surface electric fields to concentrate and transport nanoparticles continuously on a photoconductive surface. Tens of thousands of microfluidic vortices can be patterned on a  $1.3 \times 1\text{-mm}^2$  area for massively parallel manipulation of micro- and nanoscopic particles.

## II. LACE

Electroosmosis is widely used in microfluidics for liquid pumping [9]–[11]. The tangential electric field in a fluidic channel interacts with the charged ions in the double layer and generates an electrostatic force to drive the boundary liquid to flow at a slip velocity that can be calculated by using the Helmholtz–Smoluchowski equation [12]

$$\nu_{\text{slip}} = -\frac{\varepsilon\zeta E_t}{\eta} \quad (1)$$

where  $\nu_{\text{slip}}$  is the slip velocity,  $\varepsilon$  is the permittivity of the liquid medium,  $\zeta$  is the zeta potential at the interface between the liquid and the channel wall,  $E_t$  is the tangential component of electric field, and  $\eta$  is the fluidic viscosity.

Electroosmosis is usually observed in dc mode, in which the zeta potential is determined by the material property of the channel wall, the type of electrolytes, and the ionic strength. Recently, ac electroosmosis has also been applied to generate continuous dc flow by coupling the tangential electric field with the field-induced double-layer charges on electrodes [13]–[16].

Fig. 1(a) shows the device structure and the working principle of LACE. An aqueous medium containing nanoparticles and molecules of interest is sandwiched between a transparent indium tin oxide (ITO) electrode and a photoconductive electrode coated with multiple featureless layers, including a 200-nm ITO, a 50-nm n+ a-Si:H, and a 1- $\mu\text{m}$  undoped a-Si:H. An ac bias is applied to the top and the bottom ITO layers. At areas without light illumination, the undoped a-Si:H has

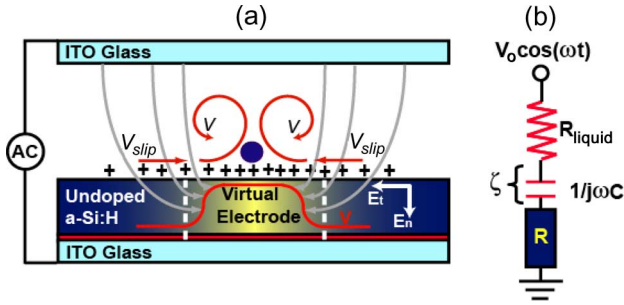


Fig. 1. Illustration of LACE mechanism. (a) A microfluidic vortex generated by a light-patterned virtual electrode through driving the double-layer charges via the tangential component of electric field. (b) The equivalent circuit model along an electric-field line. LACE operates at frequencies that are close to the double-layer relaxation frequency.

high electrical impedance compared to the liquid medium. The majority of the applied voltage drops across the a-Si:H layer. At illuminated areas, the photoconductivity of the undoped a-Si:H layer increases by several orders of magnitude, which switches the voltage to the interfacial double-layer capacitor  $C$  and the liquid layer resistor  $R$ , as shown in Fig. 1(b). By using light patterning to create virtual electrodes, electrode patterns can be changed quickly and efficiently, rendering fixed physical or chemical patterning of the electrodes unnecessary.

Because creating the boundary slip velocity requires both the tangential electric field and the charged ions at the interface, there exists an optimal ac frequency at which the product of the electric field and the interface zeta potential in (1) reaches maximum. For a frequency that is much higher than  $f_{opt}$ , the capacitor has low electrical impedance, and the bulk liquid resistor dominates. This results in a small zeta potential and a small slip velocity. For a frequency that is much lower than  $f_{opt}$ , the impedance of the capacitor is much larger than the bulk liquid layer. The electric field that can penetrate through the double layer is small, resulting in a small tangential electric field. This also yields a small slip velocity. The optimal frequency  $f_{opt} = 1/2\pi RC$  [see Fig. 1(b)] can be estimated to be

$$f_{opt} = \frac{1}{2\pi} \frac{\sigma \lambda_d}{\varepsilon L} \quad (2)$$

where  $\sigma$  is the conductivity of the liquid medium,  $\varepsilon$  is the permittivity of the liquid,  $\lambda_d$  is the double-layer thickness, and  $L$  is the gap spacing of the liquid layer. For a LACE device with 100- $\mu\text{m}$  gap spacing, a liquid conductivity of 10 mS/m, and a double-layer thickness of around 10 nm, the estimated  $f_{opt}$  is 229 Hz. The actual  $f_{opt}$  in LACE is higher than this value because the geometry factor is not considered in this estimation. In current LACE devices, the operation ac frequency is usually between 1 and 10 kHz. The liquid conductivity used for LACE operation is between 3 and 10 mS/m.

A microfluidic vortex pattern created by a virtual electrode on a LACE device is shown in Fig. 1(a). The charged ions accumulated at the interface are driven toward the center of a virtual electrode by the tangential field on the surface. This pumps the surrounding fluids to circulate around the virtual electrode. The polarity of the ions and electric field shown in Fig. 1(a) represents the situation in a half ac cycle. In the

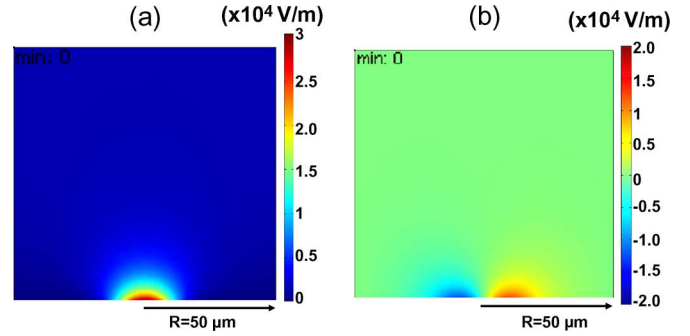


Fig. 2. Vertical- and tangential-electric-field distribution in the liquid layer induced by a virtual electrode. (a) The vertical component of electric field is symmetrical to the center of a virtual electrode and with its highest field strength in the middle. (b) The tangential component of electric field is antisymmetric to the center of a virtual electrode and with its highest electric field at the edge of a virtual electrode.

other half cycle, the polarities of both the ions and electric field change, resulting in an electrostatic force driving the fluids to flow in the same direction as in the previous half cycle. Therefore, ac electroosmosis allows an ac electrical signal to generate a dc force to pump fluids continuously in the same direction.

### III. SIMULATION OF ELECTRIC FIELD AND FLOW PATTERN

The LACE mechanism is simulated using both the electrostatic and incompressible Navier–Stokes fluidic models on FEMLAB 3.0. A dc electrostatic model is chosen to calculate the zeta potential, the tangential component of the electric field, and the slip velocity at the surface of the photoconductive layer. In the dc electrostatic simulation, the double-layer capacitor layer is represented by a conductive layer with an equivalent electrical resistance at the operation frequency. Fig. 2 shows the vertical and tangential components of electric field in the liquid layer using the following parameters: double-layer thickness—10 nm, liquid conductivity—10 mS/m, and applied bias—2 V. The impedance of the capacitor is calculated at 8 kHz. The photoconductivity in the a-Si:H layer is a Gaussian distribution with a full-width-at-half-maximum spot size of 30  $\mu\text{m}$  and a peak conductivity of 0.2 mS/m. Fig. 2(a) shows that the vertical electric field is symmetric with respect to the center of the illumination spot and has a strong gradient near the surface. The tangential electric field on the surface is antisymmetric and has its largest magnitude at the edge of a virtual electrode, as shown in Fig. 2(b). The tangential electric field and the voltage across the capacitor layer, zeta potential, are extracted from the electrostatic model to calculate the slip velocity at the interface by using (1). This slip-velocity profile is used as the boundary condition to solve the incompressible Navier–Stokes equations for the flow pattern shown in Fig. 3.

In Fig. 3, this light-induced flow circulates around the illumination spot, with the highest velocity at the edge of a virtual electrode. In the center surface of the virtual electrode, there exists a stagnant zone where the flow speed is zero, as shown in the inset in Fig. 3. Nanoparticles suspended in the

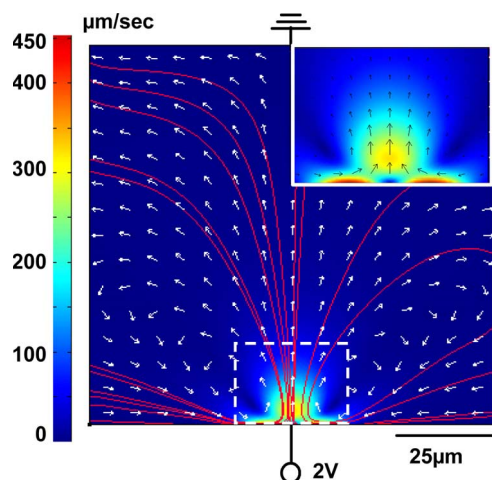


Fig. 3. Light-induced ac electroosmosis flow near a virtual electrode. The highest flow velocity exists on the surface at the edge of a virtual electrode. Owing to the symmetrical flow pattern, there exists a stagnant flow zone near the middle surface of a virtual electrode. This is where the nanoparticles are trapped.

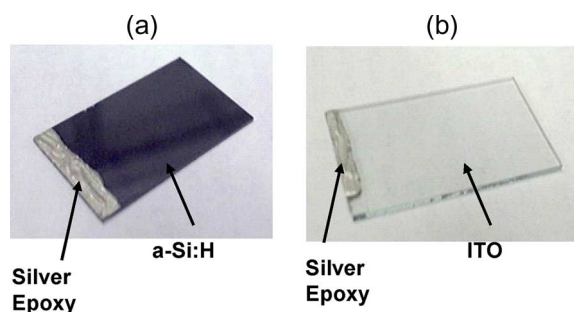


Fig. 4. Photographs of the LACE device. (a) The photoconductive a-Si:H-coated ITO glass. The a-Si:H layers at the edge are removed for electrical contact. (b) The commercially available ITO glass.

medium near the virtual electrode are circulated to the edge of the virtual electrode by viscous fluidic force and are swept into the stagnant zone.

#### IV. DEVICE FABRICATION

The fabricated LACE device is shown in Fig. 4. The photoconductive electrode that includes multiple featureless layers, a 200-nm ITO, a 50-nm n+ a-Si:H, and a 1- $\mu$ m undoped a-Si:H are deposited by using the plasma-enhanced chemical-vapor-deposition method in a foundry (Silicon Display Technology Inc., Korea). Fig. 4(a) is the fabricated photoconductive electrode. The a-Si:H at one edge is removed by reactive-ion etching ( $\text{CF}_4 + \text{O}_2$ ) to expose the bottom ITO layer for making electrical contact. Fig. 4(b) is the commercially available transparent ITO glass.

Fig. 5 shows the experimental setup constructed on a Nikon TE-2000E inverted microscope. The LACE device is placed on the observation stage. We can operate the LACE device with the photoconductive side being either up or down. For fluorescent observation, the photoconductive surface is placed on top of the ITO glass to prevent the excitation and the emission signals from being absorbed by the a-Si:H layer.

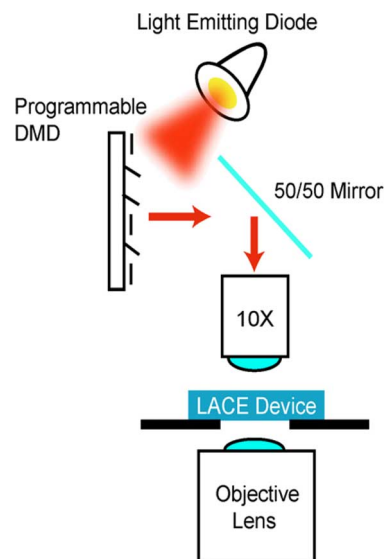


Fig. 5. Experimental setup for nanoparticle manipulation using LACE.

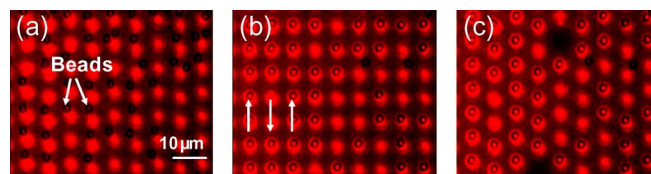


Fig. 6. Parallel trapping and transport of single 2- $\mu$ m polystyrene beads. Each trap is produced by a single DMD pixel, and the pitch is 5 pixels. There are 31 000 traps in total, which are created on a  $1.3 \times 1\text{-mm}^2$  area.

#### V. EXPERIMENT RESULTS

Using LACE mechanism, we have created 31 000 traps across a  $1.3 \times 1\text{-mm}^2$  area for trapping and transporting 2- $\mu$ m beads in parallel using a digital micromirror device (DMD) display. The illumination source is a red light-emitting diode (625-nm wavelength), and each light pixel uses 25-nW light power. Fig. 6 shows a small part of this trap array. Each trap is produced by a single DMD pixel. The spot size of each virtual electrode is 1.54  $\mu$ m, and the pitch is 8  $\mu$ m. In Fig. 6(a), the particles are randomly distributed and not yet trapped by LACE. Within a second, these particles are swept into the bright spots by microfluidic vortices induced around virtual electrodes. The spot size of the virtual electrode is small enough that each trap only accommodates one particle. The untrapped particles keep moving in the dark area until they are captured by an empty trap, as shown in Fig. 6(b). Two trapped particles can be combined together by projecting optical patterns with optical spots merging. The applied ac frequency is 1 kHz, and the bias is 4  $V_{pp}$ . The process from Fig. 6(a)–(c) takes less than 10 s. The same optical patterns can also be used to trap 1- $\mu$ m beads individually. For particles with sizes that are smaller than 1  $\mu$ m, multiple particles can be trapped in one optical spot.

Fig. 7(a) shows the concentration of 2- $\mu$ m polystyrene beads on a 20- $\mu$ m-diameter virtual electrode. These beads not only concentrate in the center of the virtual electrode but also form crystalline colloidal structures. This is because when particles

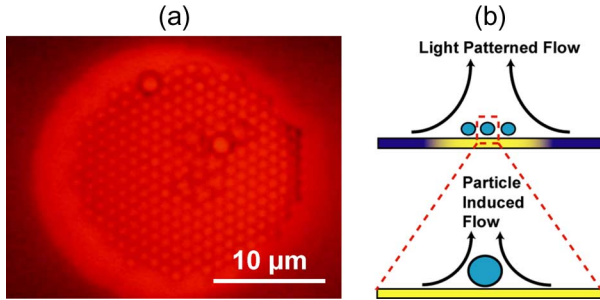


Fig. 7. (a) Polystyrene beads of 2  $\mu\text{m}$  form crystalline colloidal structures in the center of a 20- $\mu\text{m}$ -diameter virtual electrode. (b) Particles concentrated on a virtual electrode perturb the double layer and induce ac electroosmosis flow around them.

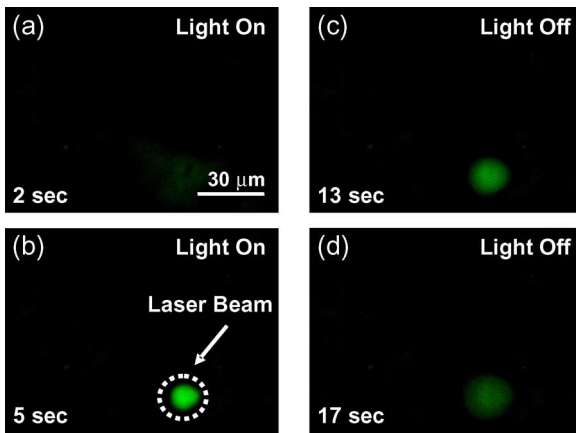


Fig. 8. Snapshots of the captured video showing the concentration and release of 200-nm fluorescent particles using LACE activated by a 5-mW 632-nm laser beam.

are circulated to the surface of a virtual electrode, they perturb the electric double layer on the electrodes and create particle-induced ac electroosmotic flows around themselves, as shown in Fig. 7(b). These particle-induced ac electroosmotic flows help these particles form compact crystalline structures. Similar phenomena have also been reported and applied for guiding the self-assembly processes of micro- and nanoscopic colloidal structures using physically patterned or light-patterned electrodes [13], [17], [18].

Fig. 8 shows the trapping and releasing of a group of 200-nm green fluorescent particles by using a 5-mW 632-nm laser beam and a 8.3- $V_{pp}$  1.6-kHz ac bias. In Fig. 8(a), the particles are dispersed in the solution, and the fluorescent signals are weak. In Fig. 8(b), the focused laser beam is turned on, and the particles are concentrated in the center of the illuminated spot. The fluorescent intensity saturates after a few seconds, indicating that the number of trapped particles has reached a maximum of this trap. The laser beam is turned off after the intensity saturates, and the concentrated particles diffuse away due to the Brownian motion, as shown in Fig. 8(c) and (d). Fig. 9(a) shows the temporal response of the fluorescent signal at the center of the illuminated spot. The saturated concentration and the time to reach this saturation are ac voltage dependent. For 4-, 6.8-, and 8.3- $V_{pp}$  biases, it takes 5.8, 2.55, and 2.19 s to reach saturation, respectively, as shown in Fig. 9(b).

These results show that a larger ac bias provides stronger ac electroosmosis flow, which can concentrate nanoparticles on the virtual electrode surface in a shorter time, and stronger vertical confinement of nanoparticles, which gives rise to the higher saturation intensity. However, the flow and the saturated concentration do not increase linearly with the applied voltage. The rise time and the saturation concentration do not have much difference between 6.8 and 8.3  $V_{pp}$ . This is because the double-layer capacitor and the zeta potential are not linear at high voltage [19].

Because light-patterned virtual electrodes can be continuously reconfigured on a featureless LACE device, this allows a light beam to concentrate and transport nanoparticles to any locations on a 2-D surface without losing them. This is difficult to achieve using physically patterned digitized electrodes because the effective trapping range between nearby electrodes may not overlap, which results in losing the trapped particles during transportation. Fig. 10 shows a continuous transportation of 200-nm fluorescent polystyrene beads on a LACE device using a 5-mW 632-nm laser beam, with a spot size of 17.6  $\mu\text{m}$ , and a 6- $V_{pp}$  1-kHz ac bias. The maximum transport speed is 7.6  $\mu\text{m}/\text{s}$ .

LACE concentration of nanoparticles can also be activated directly by the halogen or mercury lamps on a microscope. Fig. 11(a) shows the concentration of  $\lambda$ -phage DNA (Rockland Immunochemicals, Inc.) by patterning the blue fluorescent excitation illumination light with a partially closed iris ring on an inverted microscope. The illuminated spot size is around 200  $\mu\text{m}$ . It takes less than 10 s to concentrate  $\lambda$ -phage DNA molecules to what is shown in Fig. 11(a). We have also demonstrated LACE trapping of other types of nanoparticles including quantum dots (Invitrogen Inc., Qdot 565 ITK amino (PEG) quantum dots, 15–20-nm size) and 50-nm carboxylated polystyrene beads (Polysciences, Inc.), as shown in Fig. 11(c) and (d). Both of them are focused to the center of the illuminated area. Adding a dc bias introduces extra electrophoretic forces during LACE concentration process; however, they do not seem to be dominant within  $-1$ – $1$ -V dc-bias range for trapping the  $\lambda$ -phage DNA molecules and the negatively charged 50-nm polystyrene beads, as shown in Fig. 11(b) and (c).

## VI. DISCUSSION

Concentration and transportation of nanoparticles using LACE mechanism involve forces in multiple domains. Particles that are near a virtual electrode are circulated onto the photoconductive surface by viscous forces in fluid. Because the maximum slip velocity occurs at the edge of a virtual electrode, the fluidic flow forms a potential barrier to keep nanoparticles trapped in the middle of a virtual electrode from escaping the trap in the lateral direction. The slip velocity induced by ac electroosmosis can be as high as 400  $\mu\text{m}/\text{s}$  by applying a 3- $V_{pp}$  voltage [16], which is an order of magnitude higher than the diffusion speed of a 1-nm particle at room temperature. This gives LACE concentration strong lateral confinement of nanoparticles.

DEP forces play an important role in LACE concentration processes. In fact, optical patterns used to trap 2- and 1- $\mu\text{m}$

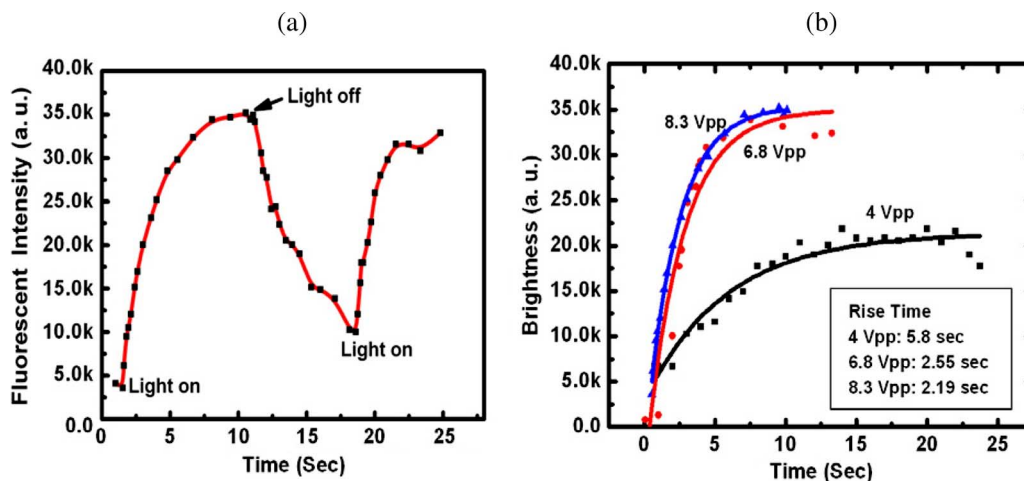


Fig. 9. (a) Fluorescent intensity at the center of the illumination spot shown in Fig. 8. LACE concentration process is reversible. (b) The transient fluorescent intensity in the center of the virtual electrode at different ac biases.

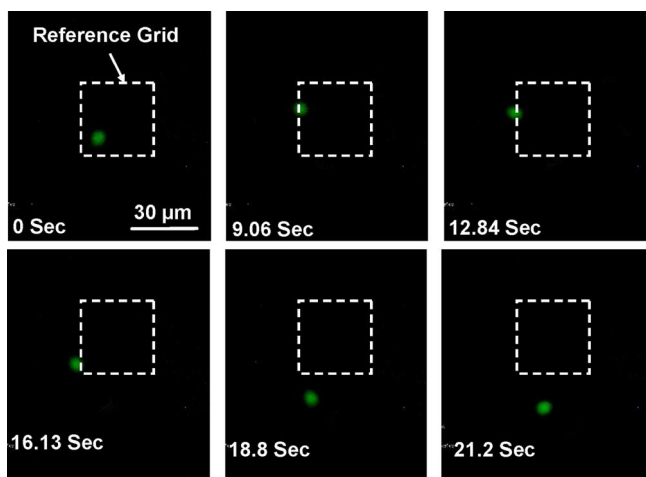


Fig. 10. LACE concentration of 200-nm fluorescent polystyrene particles using a 5-mW 632-nm scanning laser beam. The diameter of the illuminating laser spot is 17.6  $\mu\text{m}$ . The maximum transport speed is 7.6  $\mu\text{m/s}$ .

polystyrene beads in Fig. 6 cannot trap polystyrene beads that are larger than 3  $\mu\text{m}$ . Negative DEP forces at the edges of virtual electrodes are strong enough to keep the beads from being swept into the center of virtual electrodes.

Aside from DEP forces and the viscous forces induced by light-induced ac electroosmosis flow, nanoparticles trapped on the surface of virtual electrodes also perturb the electric double layer and create ac electroosmosis flow around themselves. This particle-induced ac electroosmosis flow helps trapped particles form crystalline colloidal structure, as shown in Fig. 7.

The forces that are responsible for the vertical confinement of nanoparticles could be positive DEP forces resulting from the vertical-electric-field gradient in the middle of virtual electrodes, as suggested by several groups [8], [20], [21]. However, other types of forces such as particle-induced ac electroosmosis and electrophoretic forces [8], specifically for small molecules, should also be considered for factors affecting the vertical confinement in LACE devices.

## VII. CONCLUSION

In conclusion, we have demonstrated a novel LACE mechanism that allows patterning microfluidic vortices on a featureless photoconductive hydrogenated amorphous-silicon-coated glass substrate using optical images. These light-patterned vortices, together with the self-aligned strong electric field on the surface of virtual electrodes, can concentrate and transport a variety of micro- and nanoscale particles including 2- $\mu\text{m}$ , 1- $\mu\text{m}$ , 200-nm, and 50-nm polystyrene beads;  $\lambda$ -phage DNA molecules; and quantum dots. By integrating a DMD microdisplay, we can generate 31 000 microfluidic vortices on a  $1.3 \times 1\text{-mm}^2$  area, with each vortex individually addressing a single digital micromirror pixel.

The lateral confinement of nanoparticles concentrated on the middle surface of virtual electrodes is strong because the ac electroosmosis flow at the edges of virtual electrodes can be as high as hundreds of micrometers per second, forming a strong potential barrier for nanoparticles to diffuse out of the trap through the lateral direction.

The vertical confinement of a LACE trap could involve multiple forces including positive DEP forces, particle-induced ac electroosmosis flow, and electrophoresis. The dominant force could be different for particles of different sizes. For LACE concentration of  $\lambda$ -phage DNA molecules and 50-nm negatively charged polystyrene beads, adding dc bias perturbs the LACE concentration, but the dc electrophoretic force does not seem to dominate within  $-1$ – $1$  V.

LACE provides the concentration and transportation functions for manipulating nanoparticles. However, it does not provide immobilization functions in the current version. Some surface modification steps will be necessary to treat the amorphous-silicon surface for immobilizing concentrated nanoparticles or molecules to pattern the surface. LACE has demonstrated several advantages over other techniques for nanoparticle manipulations. The light-patterned virtual electrodes can be easily reconfigured to transport concentrated nanoparticles continuously on a 2-D surface without losing them. This is a function that is difficult to achieve using

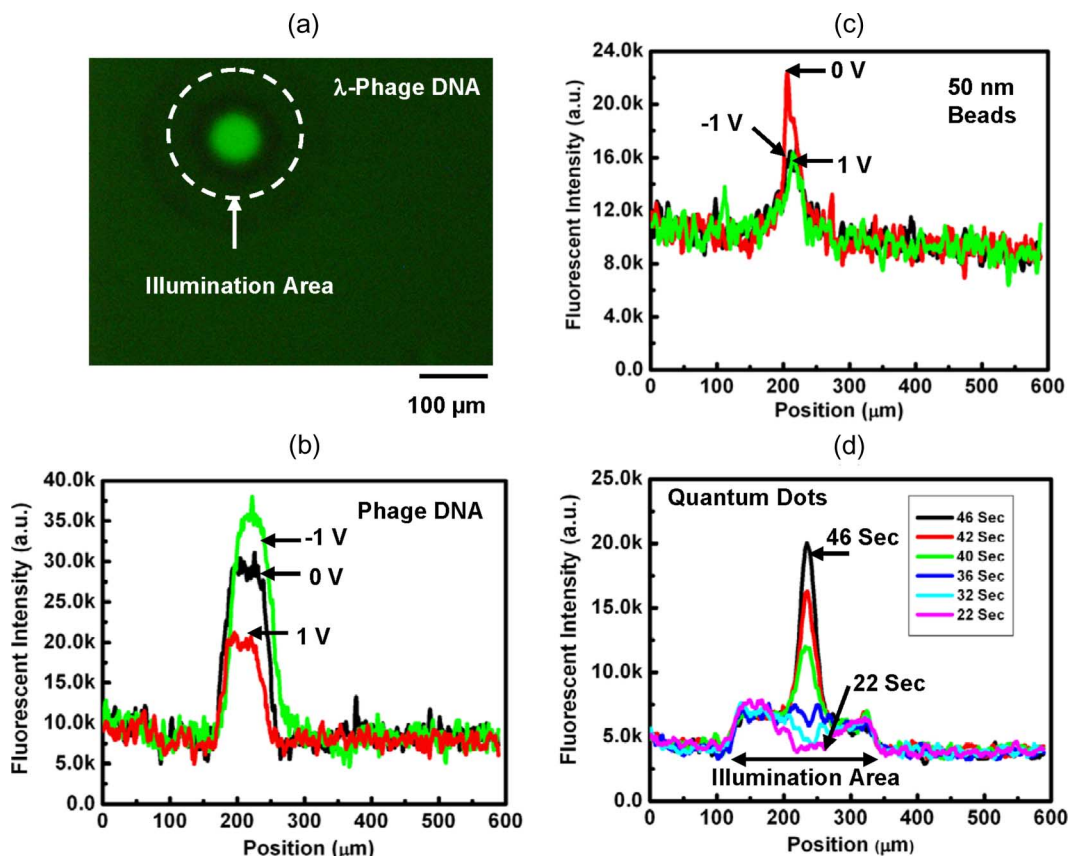


Fig. 11. LACE concentration using a circular virtual electrode patterned by partially closing the iris ring on an inverted microscope during fluorescent excitation. (a) Photograph of concentrated  $\lambda$ -phage DNA molecules. (b) and (c) Effects of adding dc biases to perturb LACE concentration of  $\lambda$ -phage DNA and 50-nm carboxylated polystyrene beads. (d) Concentrating green fluorescent quantum dots.

physically patterned digitized electrodes. The low light-intensity requirement for virtual electrode excitation allows massively parallel manipulation of tens of thousands of LACE traps using a spatial light modulator. We believe that LACE will have broad applications in the fields of nanofabrication and lab-on-a-chip systems.

## REFERENCES

- [1] A. Ashkin, J. M. Dziedzic, J. E. Bjorkholm, and S. Chu, "Observation of a single-beam gradient force optical trap for dielectric particles," *Opt. Lett.*, vol. 11, no. 5, pp. 288–290, May 1986.
- [2] D. G. Grier, "A revolution in optical manipulation," *Nature*, vol. 424, no. 6950, pp. 810–816, Aug. 14, 2003.
- [3] C. F. Chou, J. O. Tegenfeldt, O. Bakajin, S. S. Chan, E. C. Cox, N. Darnton, T. Duke, and R. H. Austin, "Electrodeless dielectrophoresis of single- and double-stranded DNA," *Biophys. J.*, vol. 83, no. 4, pp. 2170–2179, Oct. 2002.
- [4] T. B. Jones, *Electromechanics of Particles*. New York: Cambridge Univ. Press, 1995.
- [5] P. Y. Chiou, A. T. Ohta, and M. C. Wu, "Massively parallel manipulation of single cells and microparticles using optical images," *Nature*, vol. 436, no. 7049, pp. 370–372, Jul. 21, 2005.
- [6] B. G. Hosu, K. Jakab, P. Banki, F. I. Toth, and G. Forgacs, "Magnetic tweezers for intracellular applications," *Rev. Sci. Instrum.*, vol. 74, no. 9, pp. 4158–4163, Sep. 2003.
- [7] H. Lee, A. M. Purdon, and R. M. Westervelt, "Manipulation of biological cells using a microelectromagnet matrix," *Appl. Phys. Lett.*, vol. 85, no. 6, pp. 1063–1065, Aug. 9, 2004.
- [8] P. K. Wong, C. Y. Chen, T. H. Wang, and C. M. Ho, "Electrokinetic bioprocessor for concentrating cells and molecules," *Anal. Chem.*, vol. 76, no. 23, pp. 6908–6914, Dec. 2004.
- [9] H. Daiguji, P. D. Yang, and A. Majumdar, "Ion transport in nanofluidic channels," *Nano Lett.*, vol. 4, no. 1, pp. 137–142, Jan. 2004.
- [10] M. Mpholo, C. G. Smith, and A. B. D. Brown, "Low voltage plug flow pumping using anisotropic electrode arrays," *Sens. Actuators B, Chem.*, vol. 92, no. 3, pp. 262–268, Jul. 2003.
- [11] R. B. M. Schasfoort, S. Schlautmann, L. Hendrikse, and A. van den Berg, "Field-effect flow control for microfabricated fluidic networks," *Science*, vol. 286, no. 5441, pp. 942–945, Oct. 1999.
- [12] J. Lyklema, *Fundamentals of Interface and Colloid Science*, vol. 2. London, U.K.: Academic, 1991.
- [13] R. C. Hayward, D. A. Saville, and I. A. Aksay, "Electrophoretic assembly of colloidal crystals with optically tunable micropatterns," *Nature*, vol. 404, no. 6773, pp. 56–59, Mar. 2, 2000.
- [14] N. G. Green, A. Ramos, A. Gonzalez, H. Morgan, and A. Castellanos, "Fluid flow induced by nonuniform ac electric fields in electrolytes on microelectrodes. I. Experimental measurements," *Phys. Rev. E, Stat. Phys. Plasmas Fluids Relat. Interdiscip. Top.*, vol. 61, no. 4, pp. 4011–4018, Apr. 2000.
- [15] A. Ramos, H. Morgan, N. G. Green, and A. Castellanos, "AC electric-field-induced fluid flow in microelectrodes," *J. Colloid Interface Sci.*, vol. 217, no. 2, pp. 420–422, Sep. 1999.
- [16] J. P. Urbanski, T. Thorsen, J. A. Levitan, and M. Z. Bazant, "Fast AC electro-osmotic micropumps with nonplanar electrodes," *Appl. Phys. Lett.*, vol. 89, no. 14, p. 143 508, Oct. 2006.
- [17] W. D. Ristenpart, I. A. Aksay, and D. A. Saville, "Assembly of colloidal aggregates by electrohydrodynamic flow: Kinetic experiments and scaling analysis," *Phys. Rev. E, Stat. Phys. Plasmas Fluids Relat. Interdiscip. Top.*, vol. 69, no. 2, p. 021 405, Feb. 2004.
- [18] W. D. Ristenpart, I. A. Aksay, and D. A. Saville, "Electrically guided assembly of planar superlattices in binary colloidal suspensions," *Phys. Rev. Lett.*, vol. 90, no. 12, p. 128 303, Mar. 2003.
- [19] M. S. Kilic, M. Z. Bazant, and A. Ajdari, "Steric effects in the dynamics of electrolytes at large applied voltages. II. Modified Poisson–Nernst–Planck

equations," *Phys. Rev. E, Stat. Phys. Plasmas Fluids Relat. Interdiscip. Top.*, vol. 75, no. 2, p. 210 503, Feb. 2007.

- [20] M. R. Bown and C. D. Meinhart, "AC electroosmotic flow in a DNA concentrator," *Microfluidics Nanofluidics*, vol. 2, no. 6, pp. 513–523, Nov. 2006.
- [21] K. F. Hoettges, M. B. McDonnell, and M. P. Hughes, "Use of combined dielectrophoretic/electrohydrodynamic forces for biosensor enhancement," *J. Phys. D, Appl. Phys.*, vol. 36, pp. L101–L104, Oct. 2003.



**Pei-Yu Chiou** (M'05) received the B.S. degree from the Mechanical Engineering Department, National Taiwan University, Taipei, Taiwan, R.O.C., in 1998, the M.S. degree from the Electrical Engineering Department, University of California, Los Angeles, in 2004, and the Ph.D. degree from the Electrical Engineering and Computer Sciences Department, University of California, Berkeley, in 2005.

He has been with the Mechanical and Aerospace Engineering Department, University of California, Los Angeles, since 2006. His current research interests include bio-microelectromechanical systems, biophotonics, and nanophotonics.



**Aaron T. Ohta** (S'99) received the B.S. degree in electrical engineering from the University of Hawaii, Manoa, Honolulu, and the M.S. degree in electrical engineering from the University of California, Los Angeles, in 2003 and 2004, respectively. He is currently working toward the Ph.D. degree in electrical engineering at the University of California, Berkeley.

His research interests include microelectromechanical systems (MEMS) and bio-MEMS.

Mr. Ohta is the recipient of the National Science Foundation Graduate Research Fellowship.



**Arash Jamshidi** received the B.S. degree in electrical engineering from Simon Fraser University, Burnaby, BC, Canada, in 2005, and the M.S. degree from the University of California, Berkeley. He is currently working toward the Ph.D. degree at the University of California, working on optoelectronic tweezers applications in the nanoscale as part of the Integrated Photonics Laboratory Research Group.

His interests include nanotechnology, optoelectronics, and biomicroelectromechanical systems.



**Hsin-Yi Hsu** received the B.S. degree in electrical engineering from Purdue University, West Lafayette, IN, in 2005, and the M.S. degree in electrical engineering from the University of California, Berkeley, where he is currently working toward the Ph.D. degree.

His research interests include microelectromechanical systems, microfluidics, and optical systems for biomedicine applications.



**Ming C. Wu** (S'82–M'83–SM'00–F'02) received the B.S. degree in electrical engineering from National Taiwan University, Taipei, Taiwan, R.O.C., and the M.S. and Ph.D. degrees in electrical engineering and computer sciences from the University of California, Berkeley, in 1985 and 1988, respectively.

From 1988 to 1992, he was a Member of Technical Staff at AT&T Bell Laboratories, Murray Hill, NJ. From 1992 to 2004, he was a Professor with the Electrical Engineering Department, University of California, Los Angeles, where he also served as the Vice Chair for the Industrial Affiliate Program and the Director of the Nanoelectronics Research Facility. In 2004, he was with the University of California, Berkeley, where he is currently a Professor of electrical engineering and computer sciences. He is also a Codirector of the Berkeley Sensor and Actuator Center. He has published six book chapters, over 135 journal papers, and 280 conference papers. He is the holder of 14 U.S. patents. His research interests include optical microelectromechanical systems (MEMS), high-speed semiconductor optoelectronics, nanophotonics, and biophotonics.

Dr. Wu is a member of the Optical Society of America. He was a Packard Foundation Fellow from 1992 to 1997. He is the Founding Cochair of the IEEE Lasers and Electro-Optics Society (LEOS) Summer Topical Meeting on Optical MEMS (1996) and the predecessor of the IEEE LEOS International Conference on Optical MEMS. He has served on the program committees of many technical conferences, including MEMS, Optical Fiber Communication Conference, Conference on Lasers and Electro-Optics, LEOS, Microwave Photonics Conference, International Electron Devices Meeting, Device Research Conference, and International Solid-State Circuits Conference, and as a Guest Editor of two Special Issues of IEEE journals on optical MEMS.